Acta Materialia 160 (2018) 137–146

Contents lists available at ScienceDirect

Acta Materialia

journal homepage: www.elsevier.com/locate/actamat

Full length article

The role of Ni in modifying the order of the phase transition of $La(Fe,Ni,Si)_{13}$

Luis M. Moreno-Ramírez [a], Carlos Romero-Muñiz [b], Jia Yan Law [a], Victorino Franco [a, *], Alejandro Conde [a], Iliya A. Radulov [c], Fernando Maccari [c], Konstantin P. Skokov [c], Oliver Gutfleisch [c]

[a] Dpto. Física de la Materia Condensada, ICMSE-CSIC, Universidad de Sevilla, P.O. Box 1065, 41080, Sevilla, Spain
[b] Dpto. de Física Teórica de la Materia Condensada, Universidad Autónoma de Madrid, E-28049, Madrid, Spain
[c] Institut für Materialwissenschaft, TU Darmstadt, 64287, Darmstadt, Germany

ARTICLE INFO

Article history:
Received 24 July 2018
Received in revised form
27 August 2018
Accepted 28 August 2018
Available online 30 August 2018

Keywords:
Magnetocaloric effect
LaFeSi
Phase transitions

ABSTRACT

In this work, we study the effect of Ni substitution on the magnetocaloric properties of $La(Fe,Si)_{13}$ compounds. Sample quality has been optimized by a combination of induction melting and suction casting techniques, which allowed to shorten the annealing time by an order of magnitude and expand the existing range of $LaFe_{11.6-x}Ni_xSi_{1.4}$ phase with cubic $NaZn_{13}$-type structure up to $x = 0.4$. According to our Density Functional Theory calculations, Ni addition does not significantly alter the crystal structure (finding that Ni atoms occupy preferably 96i positions) as well as the total magnetic moment; both predictions are in agreement with experimental results. With increasing of Ni concentration, the transition temperature increases and the order of the phase transition changes from first to second-order type. In addition, we show that the magnetic field dependence of magnetocaloric effect enables a clear analysis of the order of phase transition even for compositions near the critical point, surpassing the accuracy of conventionally used techniques for determining the order of magnetic phase transitions (e.g. Banerjee's criterion).

1. Introduction

Magnetic refrigeration is a new technology aiming to replace the conventional chillers exploiting the gas expansion/compression cycles, which are dominating the market since 1927 when first commercial devices appeared. Most of the traditional refrigerators operate in a closed circuit, in which the condensation/evaporation of gas leads to wasted heating/cooling of a load. For magnetic refrigeration, a solid magnetic material substitutes those gas refrigerants and the expansion/compression is replaced by the application/removal of a magnetic field [1–4]. Hence, the use of non-environmental-friendly gases, such as CFC, NH_3, HCFC or HCF, responsible for greenhouse effect and ozone depletion is eliminated. Furthermore, magnetocaloric prototypes show a larger energy efficiency (60% of the theoretical limit versus 40% in typical refrigerators), which is another significant advantage of magnetic refrigeration [5].

This emerging magnetic refrigeration technology is based on the magnetocaloric (MC) effect. This effect, discovered and explained by P. Weiss in 1917 [6], is defined as the thermal response of a magnetic material upon subjected to a varying magnetic field [7–10] and is conventionally ascribed to the interactions between the magnetic and lattice subsystems. With the application of an alternating magnetic field, the entropy of the magnetic subsystem changes due to the alignment/misalignment of the magnetic moments along the direction of the magnetic field while the lattice entropy is only affected by temperature variations. Under isothermal conditions, the system undergoes a change in the total entropy (ΔS_T) that equates to the variation in the magnetic subsystem (no lattice contribution to the entropy). When the magnetic field is changed adiabatically, a variation of the material temperature (ΔT_S) results from the change in lattice entropy that compensates for the magnetic entropy change, as the total entropy is maintained constant.

A significant MC effect (i.e. large values of ΔS_T and ΔT_S at moderate magnetic field change of 1–2 T, which are used in real devices) occurs in the vicinity of a magnetic phase transition. Phase

* Corresponding author.
E-mail address: vfranco@us.es (V. Franco).

https://doi.org/10.1016/j.actamat.2018.08.054
1359-6454/

transitions are mainly classified as first (FOPT) and second-order (SOPT) phase transitions according to the Ehrenfest's classification [11]. A FOPT is characterized by a discontinuity in the first derivative of the free energy associated to a thermodynamic parameter (leading to the existence of a latent heat, coexistence of the two phases during the transition and hysteresis phenomena [12]). A SOPT is characterized by a discontinuity in the second derivative of the free energy (leading to a continuous phase transformation). With this, MC materials are categorized with the same classification. Typically, SOPT MC materials present lower MC effect than FOPT MC materials, nevertheless exhibiting a broader temperature width of MC maximum and a reversible character of the transition. The FOPT MC materials show a large MC effect but in a narrow temperature range accompanied by thermal/field hysteresis.

Nowadays, one of the most promising family of MC materials are $La(Fe,Si)_{13}$ compounds [13,14]. These compounds are compositionally based on abundant, non-critical and non-contaminant elements. From the different binary systems consisting of a rare earth element and one of the Fe, Co or Ni transition metals, only the La–Co system presents an intermetallic compound with the $NaZn_{13}$-type structure [15,16]. The large saturation magnetization and high Curie temperature of $LaCo_{13}$ made it attractive for its possible application as a permanent magnet (with limited success, as the cubic structure has no anisotropy) or as a high temperature soft magnetic material [17,18]. It is possible to obtain the $NaZn_{13}$-type structure in the $LaFe_{13}$ system by incorporating Si [19]. The cubic $La(Fe,Si)_{13}$ phase shows a temperature-induced FOPT ferro-paramagnetic transition (as well as field-induced para-ferromagnetic transition) around 200 K. The temperature and type of the transition are strongly depended on Si content [20,21]. The corresponding transition leads to an MC effect with moderate thermal hysteresis (compared to other FOPT MC materials, such as FeRh or Heusler alloys) and with associated volume change of around 1% though the crystal symmetry remains unaltered (magneto-elastic transition). Hydrogenation of the $La(Fe,Si)_{13}$ compounds produces an expansion of the $NaZn_{13}$-type unit cell that shifts the transition temperature (T_{trans}) close to room temperature (around 340 K) without decreasing the MC effect, which facilitates their application in room temperature devices [22,23].

However, it entails issues to be solved before commercialization of $La(Fe,Si)_{13}$, for example the material degradation under cycling or reducing the thermal hysteresis [24]. Its MC effect is tunable by the additions of different dopants (mainly, rare earths substitution to La or transition metals to Fe). It has been reported that elements on the left side of Fe in the periodic table, which exhibit similar atomic radius as Fe (e.g. Mn [25], Cr [26]), shift T_{trans} to lower temperatures (antiferromagnetic coupling) [27]. Conversely, those on the right side (e.g. Co [28], Ni [26]) shift T_{trans} to higher temperatures (ferromagnetic coupling) [27]. For Ni additions, the MC effect can be tuned in the same way as Co additions but the former avoids using critical raw materials and at the same time reducing material cost (Co is a critical element), which contributes to enabling commercial magnetocaloric devices.

With the aim of studying the influence of Fe substitution by Ni on the properties of $La(Fe,Si)_{13}$ magnetocaloric materials, a series of $LaFe_{11.6-x}Ni_xSi_{1.4}$ compounds were developed and characterized. The studied samples, produced by induction melting and suction casting, exhibit an extended compositional critical point of SOPT of $x_{critical} = 0.21$ (leading to a 2.6-fold extension compared to previously reported similar alloys [26]) together with high sample homogeneity and amount of $NaZn_{13}$ phase. Density Functional Theory (DFT) calculations show that the $NaZn_{13}$-type crystal structure is retained with Ni substitutions, in agreement with experiments. The order of the phase transition is also studied using the Banerjee's criterion and two other methods based on field dependence of MC effect (one based on the Bean and Rodbell model [29] and a recent proposed quantitative criterion using the field exponent [30]). The latter two techniques are shown to successfully determine the order of phase transitions for all compositions and even address for compositions near the compositional critical point of SOPT, which is challenging for such materials exhibiting a gradual crossover from FOPT to SOPT.

2. Experimental and methods

$LaFe_{11.6}Si_{1.4}$ compound, which was demonstrated that it underwent a FOPT [31], was chosen as the parent composition. In order to investigate influence of Ni on the MC effect of this compound, 20 g of material, each with nominal compositions of $LaFe_{11.6-x}Ni_xSi_{1.4}$ ($x = 0$, 0.1, 0.2, 0.3 and 0.4) were produced by induction melting from pure elements. To remove possible oxide phases in the elements, La was initially cleaned by arc melting prior to being induction melted with other elements. It was reported that the shape and cooling rate influence the annealing time for $La(Fe,Si)_{13}$ compounds, which consequently affect the amount of the $NaZn_{13}$-type structure phase (denoted as 1:13 phase) [32]. To ensure homogeneity, the samples, encapsulated in quartz tubes under Ar atmosphere, were subsequently annealed at 1050 °C for 3 h. The annealed ingot was then further segmented into different pieces for subsequent suction casting (using a rectangular mold of $10 \times 4 \times 0.5\ mm^3$). A 9 wt. % excess of La was also added to compensate its vaporization during the melts. Suction casted samples were then annealed (wrapped in Mo foil and sealed in quartz tubes) in a resistance tube furnace at 1100 °C for 24 h to obtain high amount of the desired 1:13 phase.

Microstructural characterization and average bulk compositional quantification of the samples were performed using a Philips XL30 FEG scanning electron microscope equipped with energy-dispersive X ray system (SEM/EDX). The X-ray diffraction (XRD) of the pulverized samples were collected at room temperature using a Stoe Stadi P instrument in transmission mode with Molybdenum $K\alpha_1$ source radiation ($\lambda = 0.70930$ Å). Rietveld refinement of the XRD patterns was performed using TOPAS Version 6.0 software.

Magnetization measurements were performed with a vibrating sample magnetometer (standard option of a Quantum Design Physical Properties Measurement System, PPMS). The magnetic field was applied along the length of the suction casted plates to minimize contributions from the demagnetizing factor (further details in Results and discussion section). From isothermal magnetization (M) curves measured at different temperatures, the isothermal entropy change (ΔS_T) was calculated numerically indirectly using the Maxwell relation according to [33]:

$$\Delta S_T(T,H) = \mu_0 \int_0^H \left(\frac{\partial M}{\partial T}\right)_{H'} dH', \tag{1}$$

where the initial magnetic field is fixed as 0. The adiabatic temperature change (ΔT_S) was directly measured in a home-built experimental set-up whereby the sample was thermally isolated to ensure adiabatic conditions during the variation of the magnetic field (more information can be found in Ref. [34]). As FOPT MC materials can exhibit thermal hysteresis, a special characterization protocol for erasing the thermal and magnetic history of the samples has been applied in order to appropriately measure their isothermal magnetization curves and correctly apply the Maxwell relation for ΔS_T calculations [24,35]. A power law for the field dependence of ΔS_T (in the form of $\Delta S_T \propto H^{n(T,\Delta H)}$) is assumed

[36,37]. The local field dependence exponent n was calculated from ΔS_T data as:

$$n(T,H) = \frac{d\ln(\Delta S_T)}{d\ln(H)} . \quad (2)$$

In addition, Density Functional Theory (DFT) calculations were performed to unveil at atomic level the structural, electronic and magnetic properties of $LaFe_{11.5-x}Ni_xSi_{1.5}$ compound series, using a plane-wave basis set as implemented in the VASP package [38]. This composition is one of the closest that can be generated using the selected unit cell for the $NaZn_{13}$-type crystal. Although the Si content slightly deviates from the experimental compound investigated in this work, $LaFe_{11.5}Si_{1.5}$ also shows a FOPT and the effects of Ni additions should be similar for both cases. An energy cutoff of 335 eV was considered to build the plane-wave basis set, which was proved to accurately describe such compounds [39,40]. The projected augmented wave method [41,42] was employed for the pseudopotentials of all species involved and the Perdew-Burke-Ernzerhof (PBE) functional [43] was chosen to reproduce the exchange and correlation electronic interactions. The four constituent metals were separately tested by calculating simple bulk structures to ensure a good agreement of the obtained lattice parameters.

Following a conjugate gradient algorithm, to study their equilibrium configurations all the structures subjected to ionic relaxations were considered, starting from the same parent unit cell ($NaZn_{13}$-type) with a lattice parameter of 11.488 Å (see Results and Discussion section for further details about the cell). Although no restrictions in the cell volume were imposed during these relaxations, no significant distortions from the initial cubic symmetry are observed in the final structures. The convergence criterion to complete the structural minimization process was that forces upon atoms must be less than 0.005 eV/Å while a cutoff of 10^{-6} eV was established to achieve electronic self-consistency. Due to the large size of the cell, the reciprocal space was sampled using a $3 \times 3 \times 3$ Monkhorst-Pack grid [44]. To explore magnetic and electronic properties, collinear spin polarization was required for all calculations and the Vosko-Wilk-Nusair interpolation [45] was used to resolve the on-site magnetism at atomic level. Due to the strong ferromagnetism of this material, it is necessary to start from an initial high magnetic moment configuration, which in our case was 3.5 Bohr magnetons per Fe atom. Both magnetic and electronic features were evaluated using a thinner k-point grid of 4×4x4 and a Gaussian broadening of 0.1 eV, starting from the converged structures.

3. Results and discussion

Fig. 1 shows the back scattered electron (BSE) images for the Ni-containing $LaFe_{11.6-x}Ni_xSi_{1.4}$ samples. Bright spots correspond to $La_1Fe_1Si_1$ phase (P4/nmm), dark ones to α-Fe phase (Im-3m) and the gray ones to the desired 1:13 phase ($NaZn_{13}$-type, Fm-3c). For all studied compositions, BSE images show a homogenous structure with the main phase of the desired 1:13 stoichiometry. Almost negligible α-Fe impurities were observed for samples with low Ni contents of $x = 0.1$ and 0.2 (while some minor amounts of α-Fe was reported for similar alloys in the literature [46]). Some bright spots of $La_1Fe_1Si_1$ phase can be noticed, which could be due to the excess La added for suction casting. The dark spots corresponding to α-Fe phase become more noticeable with increasing Ni concentration for higher Ni contents ($x = 0.3$ and 0.4), although the high amount of the obtained 1:13 phase with compositions close to the nominal shows an extension of the solid solubility limit previously ascribed to Ni [47]. In addition, the compositional analysis by EDX (Table 1) shows a good agreement between the measured and nominal compositions with only slight deviations for higher Ni content. A further examination of the latter samples shows that the Ni/Fe ratio is the highest in the $La_1Fe_1Si_1$ phase than in α-Fe and 1:13 phases, indicating a preferential segregation of Ni in the La-rich phase.

Fig. 2 shows the XRD spectra for $LaFe_{11.6-x}Ni_xSi_{1.4}$ samples. It can be seen that the samples mainly consist of 1:13 phase and trace amounts of α-Fe and $La_1Fe_1Si_1$ phases are also detectable, which agree with our BSE results. In addition, minor peaks corresponding to α-Fe phase become more evident with higher Ni content, especially for $x = 0.3$ and 0.4. The results from the Rietveld refinement of the different XRD spectra and the goodness of fit (GoF) are tabulated in Table 2, in which all the GoF values close to 1 (ideal case) are observed. The amount of α-Fe increases with Ni content, showing large increments of 10.4 and 7.1 wt.% for samples with $x = 0.3$ and 0.4, which is consistent with microstructure presented in Fig. 1. Ni additions do not modify the $NaZn_{13}$-type structure though the lattice parameter decreases with increasing Ni content at a rate of −0.0018(6) Å (at.% Ni)$^{-1}$ (also shown in the compositional dependence of lattice parameter plotted in Fig. 3a).

In addition to experimental investigation, the crystal structure of related $LaFe_{11.5-x}Ni_xSi_{1.5}$ alloy series was studied using DFT calculations. They were performed using the same parent unit cell ($NaZn_{13}$-type) with periodic boundary conditions to represent the cubic symmetry (Fm-3c) of the crystal structure of $LaFe_{11.5-x}Ni_xSi_{1.5}$. It contains a total of 112 atoms (8 formula units) distributed in three nonequivalent Wyckoff positions (8a, 8 b and 96i) as depicted in Fig. 3b. While the 8 La atoms occupy the 8a positions, Fe atoms are located either at 8 b or 96i sites, giving rise to two chemically different iron species, Fe−I and Fe-II respectively. Since most of the studies [48–50] assume that the incorporation of Si atoms preferentially or exclusively takes place on 96i sites, we have randomly replaced 12 Fe-II by Si atoms in order to obtain the stoichiometric $LaFe_{11.5}Si_{1.5}$ compound, which serves as the starting point ($x = 0$) for the subsequent Ni incorporation. With this aim, we replaced additional Fe-II atoms (from 1 to 4) by Ni atoms, leading to the series $x = 0.125$, $x = 0.25$, $x = 0.375$ and $x = 0.5$, in agreement with the compositions of experimental samples. It is worth noting that this unit cell is large enough to allow an approximate random distribution of silicon and nickel substitutions. The preferential incorporation of Ni atoms at the 96i sites is also considered for other two calculations: Ni replacing a single Fe atom from the 96i and 8 b positions. The results pointed out a slightly more energetically favorable configuration (0.13 eV per unit cell) for the first choice. Taking into account the intense annealing carried out on the samples during the synthesis, we can consider that Ni atoms will finally exclusively incorporate at the 96i positions. In this sense, Ni substitution behaves very similar to the case of Co, which has been already studied by neutron diffraction [51]. Small distortions from the cubic symmetry in the equilibrium structures indicate that the original $NaZn_{13}$-type crystal structure is retained upon Ni substitutions, indicating that the substitution of Ni atoms has a very small impact on the parent crystal structure, in agreement with experimental results. The minimal reduction of the lattice parameter with increasing Ni content (Fig. 3a) also agrees with XRD results while a noticeable increment in the mass density is observed due to the higher atomic mass of Ni compared to lighter Si (see Table 3 for details).

Fig. 4 shows experimental results of the temperature dependence of the normalized magnetization (with respect to the magnetization at 170 K) at 0.05 T for the set of samples. It can be observed that the temperature span of the transition becomes broader and shifts to higher temperatures as Ni content increases. From the normalized representation, it is possible to estimate the amount of α-Fe from the high temperature range of the curves. These obtained values are in good agreement with those obtained

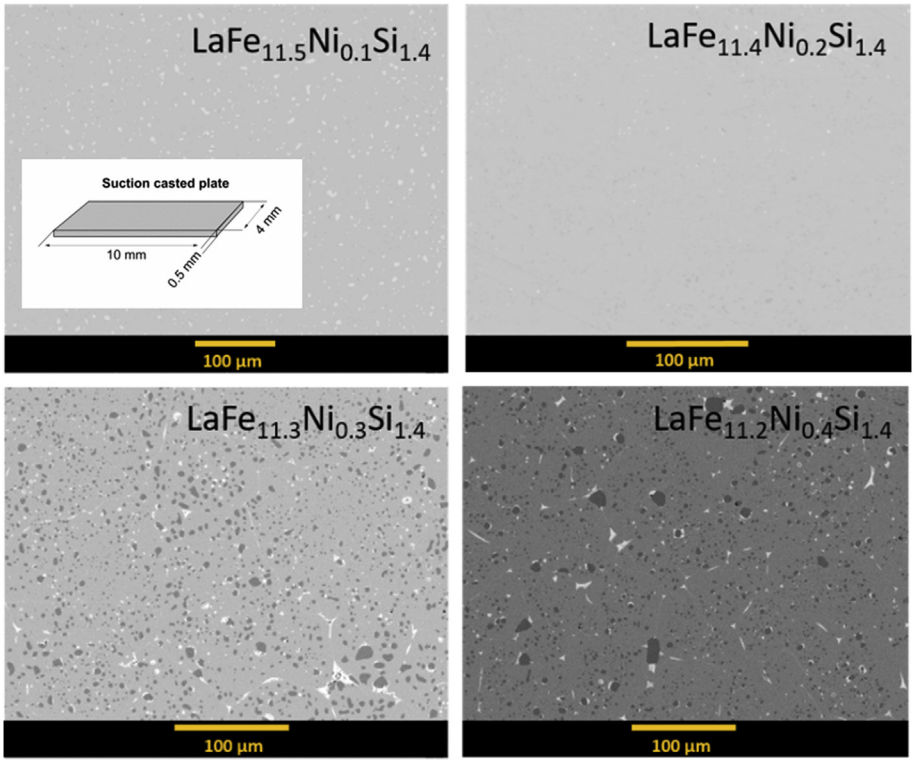

Fig. 1. BSE images for the set of $LaFe_{11.6-x}Ni_xSi_{1.4}$ series and schematic representation of suction casted plate dimensions.

Table 1
Compositional EDX analysis for the 1:13 phase in the different samples.

Sample	1:13 phase composition
$LaFe_{11.6}Si_{1.4}$	$La_{1.00(3)}Fe_{11.2(4)}Si_{1.45(12)}$
$LaFe_{11.5}Ni_{0.1}Si_{1.4}$	$La_{1.00(3)}Fe_{11.2(2)}Ni_{0.10(2)}Si_{1.42(12)}$
$LaFe_{11.4}Ni_{0.2}Si_{1.4}$	$La_{1.00(2)}Fe_{11.1(2)}Ni_{0.18(3)}Si_{1.44(12)}$
$LaFe_{11.3}Ni_{0.3}Si_{1.4}$	$La_{1.00(3)}Fe_{10.9(2)}Ni_{0.26(3)}Si_{1.50(12)}$
$LaFe_{11.2}Ni_{0.4}Si_{1.4}$	$La_{1.00(3)}Fe_{10.9(2)}Ni_{0.33(3)}Si_{1.54(12)}$

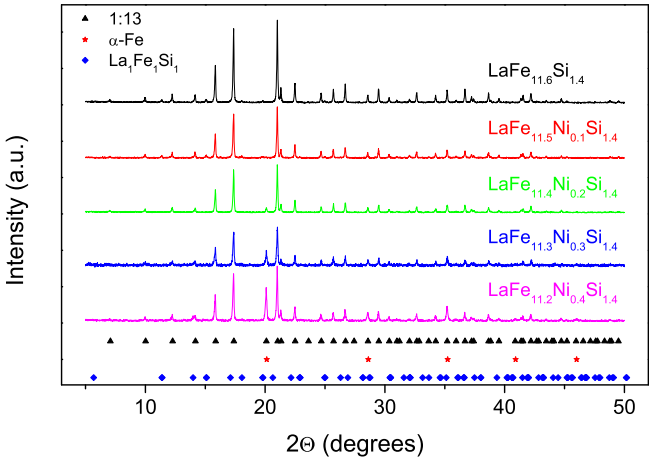

Fig. 2. XRD spectra for the $LaFe_{11.6-x}Ni_xSi_{1.4}$ series.

from the Rietveld refinement of the XRD spectra and BSE images, revealing the high homogeneity of the produced samples (as different parts and different plates have been taken into account to perform the different analyses). Magnetization values of the 1:13 phase for the different samples are slightly modified with Ni additions. Removing the α-Fe effect in magnetization curves (from the fitting of the paramagnetic tail of the data) it can be observed that the spontaneous magnetization at 180 K for the 1:13 phase slightly decreases as the Ni content increases at a rate of 7.7(2.2) emu g^{-1} (at.% Ni)$^{-1}$, although the presence of α-Fe prevents any further analysis. The transition temperature (T_{trans}) is determined as the temperature for which the derivative of magnetization with respect to temperature is maximum (shown in the inset of Fig. 4). It can be observed that T_{trans} phenomenologically follows an monotonous increase with increasing Ni content (fitted to a power law of the form $T_{trans} = a+bx^c$ with $a = 192.6(5)$, $b = 159(17)$, $c = 2.19(13)$ and $r^2 = 0.998$).

Further analysis of the magnetic behavior using spin polarized DFT calculations was performed to resolve the on-site magnetic moments of individual atoms and to provide additional information about the ferromagnetic state of these alloys. For the parent $LaFe_{11.5}Si_{1.5}$ compound a total magnetic moment per formula unit (f.u.) of 24.61 μ_B was calculated. Using crystallographic data of Table 3 a saturation magnetization of 166.9 emu g^{-1} is obtained. Fe atoms are responsible for the strong ferromagnetic behavior of this compound, displaying average magnetic moment of 2.24 μ_B (Fe-II) and 1.83 μ_B (Fe–I) per atom. Conversely, Si and La atoms show a slight antiparallel coupling with residual magnetic moment per atom of −0.10 μ_B and −0.21 μ_B respectively. These results are in good agreement with previous calculations [39,50] and reported experiments of neutron scattering [49] and Mossbauer spectroscopy [52].

In the case of partial substitution of Fe-II by Ni atoms, a slight monotonic reduction in the total magnetic moment per f. u. (and saturation magnetization) of ~1 μ_B with increasing Ni concentration was found (from 24.61 μ_B to 23.85 μ_B, see Table 3). The atomic on-site magnetic moment calculated from spin-polarized DFT is presented in Fig. 5 and it shows no relevant changes in the magnetic

Table 2
Lattice parameters of $NaZn_{13}$-type phase, phase proportions and goodness of fit (GoF) obtained for the $LaFe_{11.6-x}Ni_xSi_{1.4}$ series determined from Rietveld refinement.

Sample	a [$LaFe_{13}$] (Å)	1:13 (wt.%)	α-Fe (wt.%)	LaFeSi (wt.%)	GoF
$LaFe_{11.6}Si_{1.4}$	11.49043(13)	97.9	0.2	1.9	1.35
$LaFe_{11.5}Ni_{0.1}Si_{1.4}$	11.49179(16)	96.9	0.9	2.3	1.17
$LaFe_{11.4}Ni_{0.2}Si_{1.4}$	11.48836(15)	96.2	3.8	0	1.26
$LaFe_{11.3}Ni_{0.3}Si_{1.4}$	11.4884(3)	84.9	14.2	0.9	1.01
$LaFe_{11.2}Ni_{0.4}Si_{1.4}$	11.4857(5)	77.6	21.3	1.1	1.10

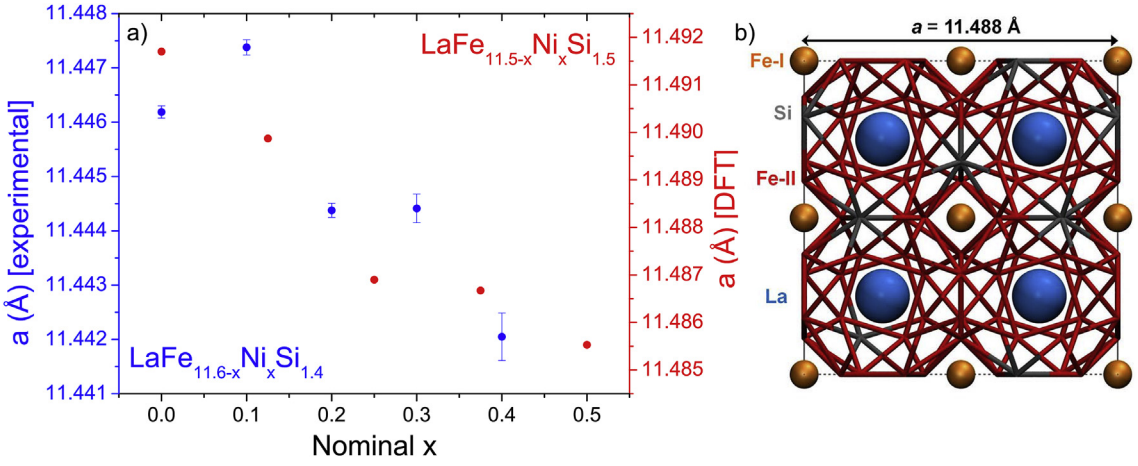

Fig. 3. a) Lattice parameter obtained from Rietveld refinement and DFT calculations for different Ni concentrations. b) Side view along de the (100) face of the unit cell of $LaFe_{11.5}Si_{1.5}$ crystal structure (space group Fm-3c) represented with a ball-and-stick model. La atoms (blue) occupy 8a positions, Fe-I (orange) 8 b sites while Fe-II and Si atoms (depicted with red or gray bonds) distribute randomly on 96i sites. (For interpretation of the references to colour in this figure legend, the reader is referred to the Web version of this article.)

Table 3
Lattice parameters, mass densities, magnetic moment per formula unit and saturation magnetization obtained from DFT calculations for the $LaFe_{11.5-x}Ni_xSi_{1.5}$ alloys.

Alloy	a (Å)	Density (g cm^{-3})	μ (μ_B)	M_S (emu g^{-1})
$LaFe_{11.5}Si_{1.5}$	11.4473	7.291	24.61	166.9
$LaFe_{11.375}Ni_{0.125}Si_{1.5}$	11.4457	7.297	24.40	165.4
$LaFe_{11.25}Ni_{0.25}Si_{1.5}$	11.4431	7.305	24.16	163.8
$LaFe_{11.125}Ni_{0.375}Si_{1.5}$	11.4429	7.309	24.04	162.8
$LaFe_{11}Ni_{0.5}Si_{1.5}$	11.4419	7.314	23.85	161.5

moment distribution of the original $LaFe_{11.5}Si_{1.5}$ species when Ni atoms are introduced. As the mean values per species remain essentially constant, the reduction of the total magnetization is attributed to the presence of Ni atoms (green bars in Fig. 5). They display a much lower magnetic moment compared to those of Fe-II atoms, with a mean magnetic moment per atom ranging from 0.4 μ_B to 0.5 μ_B, depending on the particular compound. Hence, the magnetic moments of Fe-II and Ni atoms are observed to be very similar to those of their corresponding metallic states [53]. Therefore, a reduction in the total magnetic moment per unit f. u. of ~0.2 μ_B [emerging from (2.2–0.4)/8] per Ni atom is expected (see Table 3).

The magnetic structure is further studied at atomic-scale from the various atomic contributions to the total electronic density of states (DOS), which is shown in Fig. 6. Each curve represents the accumulated projected DOS of each atom type. A strong peak contributed by La atoms is observed on empty states (E-$E_F \approx 3$ eV) while those from Fe–I and Si atoms are less significant. As expected, the dominant contribution comes from Fe-II atoms, which are responsible for the permanent magnetic moments: for e.g., remarkable discrepancies are observed between up and down DOS at E-$E_F \approx -3$ or $+2$ eV for all compositions. With the partial substitution by Ni atoms, these differences decrease with Ni content though a strong ferromagnetic behavior is preserved as the Ni/Fe ratio is still small. For low Ni content, the contribution of Ni atoms (magenta lines) to the total DOS is limited but different from that of Fe-II. Now the main mismatch between up and down spins is near E-$E_F \approx -2$ eV but in a much less accused way. This strong difference in the electronic structure between Fe-II and Ni atoms suggest for the observed variation in the magnetic properties of $LaFe_{11.5-x}Ni_xSi_{1.5}$ despite that similar total magnetic moments are obtained with varying Ni content. In the frame of DFT calculations, it is very challenging to extract quantitative information about the transition temperatures but both experimental [54] and theoretical results [55] point out that the magnetic exchange energy of Ni is clearly stronger than that of Fe. Thus, a shift of the transition temperatures to higher temperatures would be expected after partial substitution of Fe-II atoms by Ni atoms. At the mean field level, the Ni–Ni exchange interactions become more evident especially for higher Ni concentration. This is equivalent to what has been observed for Co substitution [13,56,57].

Fig. 7 (a) and (b) show the experimentally obtained temperature dependences of ΔS_T and ΔT_S (at $\mu_0\Delta H = 1.9$ T), respectively, for the different samples. For ΔS_T, it can be observed that the maximum ($\left|\Delta S_T^{pk}\right|$) decreases with Ni content at a rate of 5.8(6) J kg^{-1} K^{-1} (at.% Ni)$^{-1}$ ($r^2 = 0.95$). Moreover, the $\left|\Delta S_T^{pk}\right|$ curves for x = 0 and x = 0.1 (despite a slight reduction of $\left|\Delta S_T^{pk}\right|$ observed for the latter) maintain abrupt low temperature tails that drastically change into a gradual type for higher Ni content ($x \geq 0.2$). In addition, the corresponding temperatures of $\left|\Delta S_T^{pk}\right|$, $T_{\Delta S_T}^{pk}$, shift to higher temperatures with Ni additions, while the width of the curves becomes larger (the full width at half maximum (FWHM) varies from 8.6 to

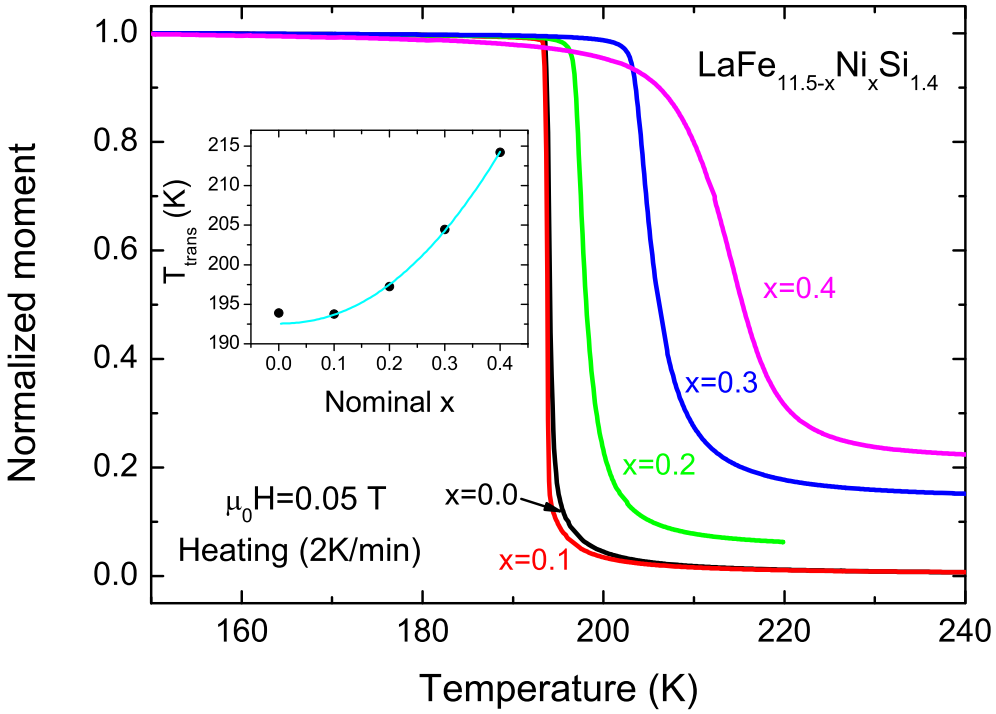

Fig. 4. Normalized magnetization (with respect to magnetization at 150 K) at 0.05 T and calculated transition temperature (inset) for the for the $LaFe_{11.6-x}Ni_xSi_{1.4}$ series.

25.7 K for the samples with x = 0 and 0.4, respectively). In the case of ΔT_S in Fig. 7b, the maximum ΔT_S decreases for x = 0.1 despite retaining a similar shape of $\Delta T_S(T)$ curve as that of x = 0 sample. Similar features as those in Fig. 7a are observed: the shapes of $\Delta T_S(T)$ curves become gradual for x ≥ 0.2, the maximum ΔT_S values reduce at a rate of 1.47(13) K (at.% Ni)$^{-1}$ ($r^2 = 0.97$), $T^{pk}_{\Delta T_S}$ shift to higher temperatures with Ni additions, and the FWHM of the peak increases with Ni content (from 5.3 to 25.7 K for the samples with x = 0 and 0.4, respectively). $\Delta T_S(T)$ curves were measured using increasing (heating) and decreasing (cooling) temperature protocols and no significant thermal hysteresis was observed for all the studied samples.

It should be noticed that, for this analysis, the effect of the demagnetizing factor have been checked. The demagnetizing factor was determined from the inverse of M vs H slope using M_H curves measured at low fields and temperatures well below the transition. The demagnetizing factor of x = 0 sample is estimated as 0.0927(3) (this value is used for the whole studied series as all the samples have similar shapes). The recalculation of ΔS_T values considering the demagnetizing factor and using the internal field instead ($H_{int} = H - NM$) results in a 2% difference in $\left|\Delta S^{pk}_T\right|$, indicating that a negligible effect on ΔS_T (and therefore ΔT_S).

To estimate the cooling power of the compounds we calculate the minimal coefficient of refrigerant performance (CRP_{min}) according to [58], whereby the temperature difference between the hot and cold reservoirs is approximated as ΔT^{pk}_S instead of the FWHM of ΔS_T curve. The CRP_{min} values decrease with Ni additions (from $CRP_{min} = 3.1$ to 0.2 for $LaFe_{11.6}Si_{1.4}$ and $LaFe_{11.2}Ni_{0.4}Si_{1.4}$, respectively). This cannot be ascribed to the presence of α-Fe observed for higher Ni content samples since the α-Fe transition is well above that of $LaFe_{13}$ phase and its mass fraction is negligible in comparison with the decrease of CRP_{min}. In addition, as both experimental and DFT calculations show no drastic alteration to overall magnetization with Ni additions, it is unlikely to attribute magnetization to the reduction in MC effect with increasing Ni content. Hence, the alteration of the nature of the phase transition could arise as responsible for this change, which is also compositional dependent.

To study how the order of the phase transitions of the samples changes with Ni concentration, two methods based on the field dependence of MC data were used. These methods do not need any fitting procedure, assumptions of the material's nature or extensive data analysis. The field dependence of ΔS_T adopts a power law expression as $\Delta S_T \propto H^n$, and its exponent n at the transition temperature is correlated to the critical exponents of the material in the form of $n(T_{trans}) = 1 + (1 - \beta^{-1})\delta^{-1}$ (where the critical exponents β and δ give the temperature dependence of M at zero field and the field dependence of M at T_{trans}, respectively) [37]. For SOPT materials with long range interactions, the values of $n(T_{trans})$ are typically similar to those determined using critical exponents for mean field model ($n(T_{trans}) = 0.67$). On the other hand, for short range interactions, the typical values are close to Heisenberg or 3D-Ising models (0.63 and 0.57, respectively). For the $n(T_{trans})$ of SOPT, there exists a lower compositional limit corresponding to the case where the material transits from SOPT to FOPT and this point is called the compositional critical point of SOPT (denoted as "tricritical point" by some authors). According to theoretical considerations, the values of the critical exponents at this critical point yield $n(T_{trans}) = 0.4$ [59]. For FOPT, although the material does not exhibit a critical region, the $\Delta S_T(H)$ in high fields lead to $n(T_{trans})$<0.4 when using the Bean and Rodbell model [60]. This is also experimentally observed for other $La(Fe,Si)_{13}$ series [21]. Therefore, there is a clear criterion to identify SOPT and FOPT MC materials based on the values of $n(T_{Trans})$ when materials can be described with the Bean and Rodbell model (e.g. $La(Fe,Si)_{13}$ compounds).

To clearly distinguish the order of the phase transition and also to find the compositional critical point of SOPT, the field dependence exponent n of the studied $LaFe_{11.6-x}Ni_xSi_{1.4}$ series is plotted as a function of temperature for $\mu_0\Delta H = 1.9$ T (main panel of Fig. 8). The $n(T_{Trans})$ as a function of Ni content is presented in the inset of

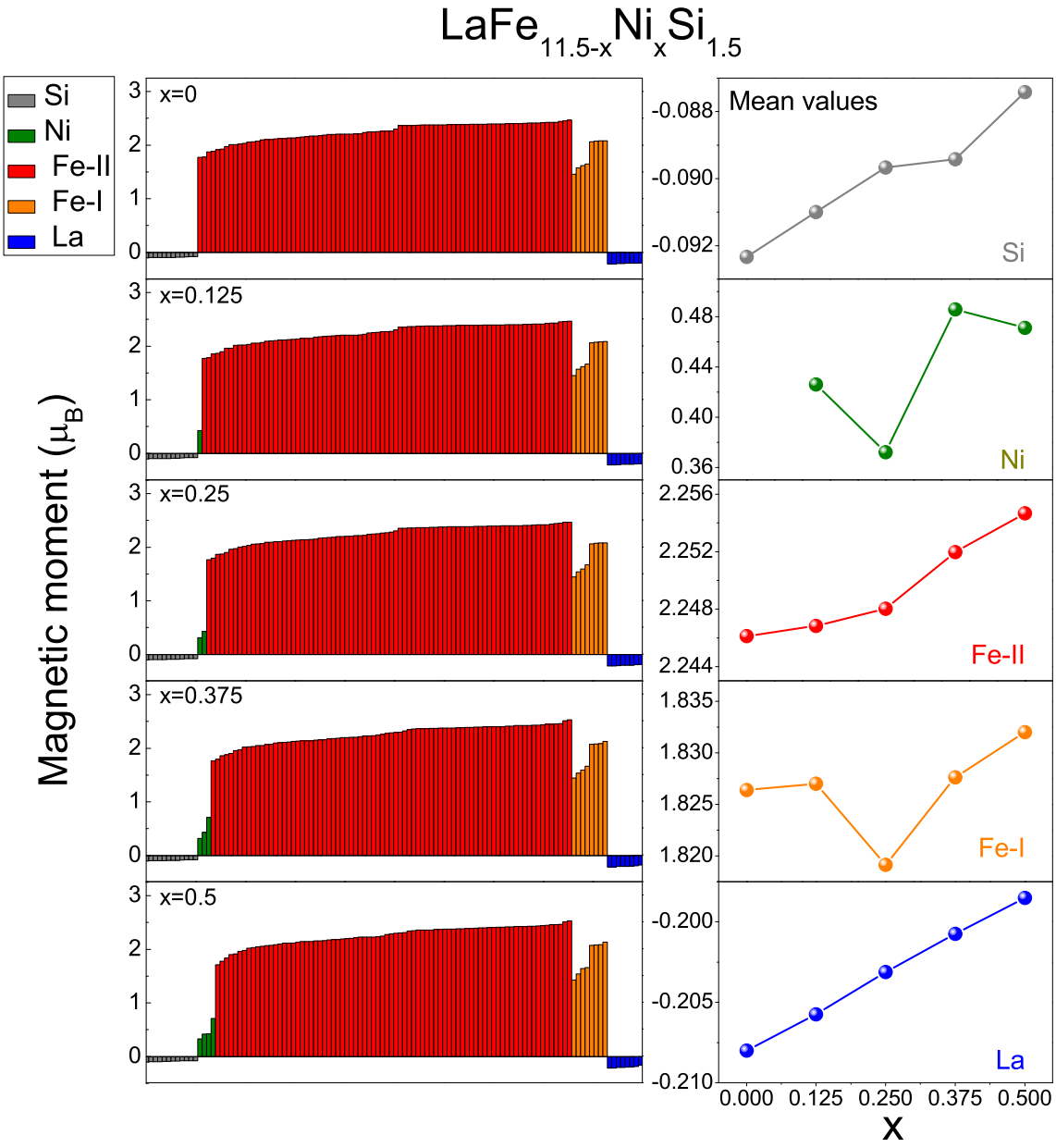

Fig. 5. Left) Atomic on-site resolved magnetic moment obtained with spin-polarized DFT for the 112 atoms of the unit cell in the $LaFe_{11.5-x}Ni_xSi_{1.5}$ compound as a function of Ni content. Right) Mean values of the moments per species in the different compounds.

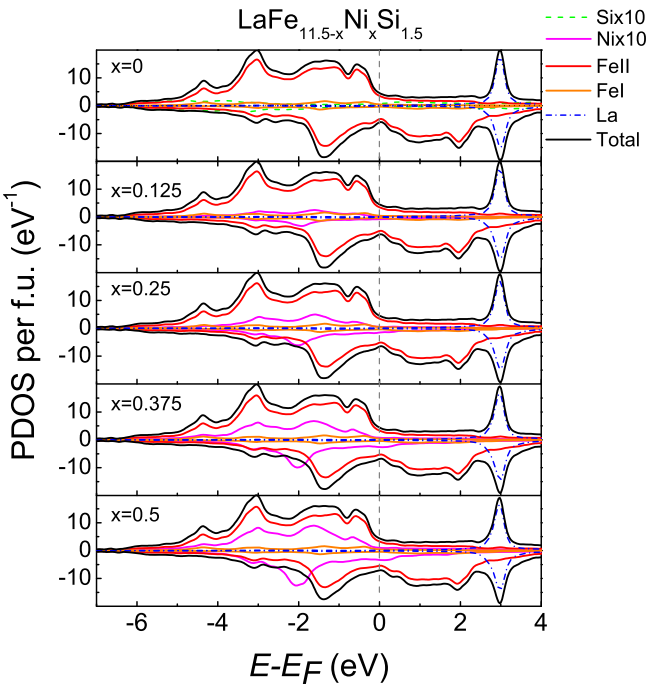

Fig. 6. Evolution of the Projected Density of States per species in the $LaFe_{11.5-x}Ni_xSi_{1.5}$ alloys. Notice that Si contribution is only shown for x = 0 and it remains unaltered in the other compositions.

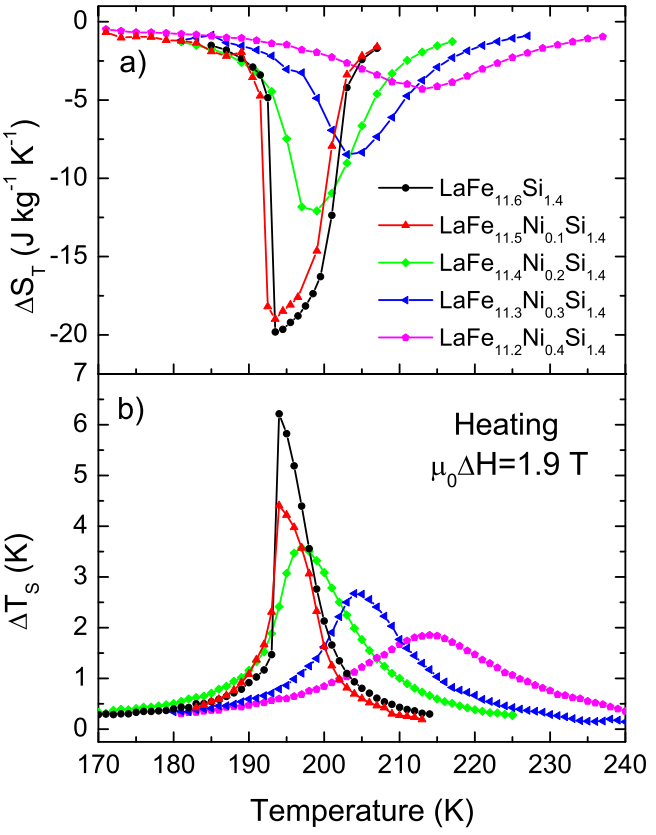

Fig. 7. a) Temperature dependence of the isothermal entropy change (ΔS_T) and b) adiabatic temperature change (ΔT_S) while heating for the $LaFe_{11.6-x}Ni_xSi_{1.4}$ series (at $\mu_0\Delta H = 1.9$ T).

Fig. 7. Although the demagnetizing effect on ΔS_T curves has been earlier shown to be negligible in this study, it is being considered for exponent n as it was reported to affect n more significantly than the former [61–63]. It can be observed that samples with x = 0, 0.1 and 0.2 show $n(T_{trans})$<0.4 values, indicating they undergo FOPT. On the other hand, larger $n(T_{trans})$ values (above 0.4) are observed for x = 0.3 and 0.4, indicating they undergo SOPT. Also, the compositional critical point of SOPT corresponding to a Ni content is predicted as x = 0.21 (where it is assumed a linear interpolation between the different points). The presence of α-Fe could contribute to increasing the values of $n(T_{trans})$ for higher Ni-containing samples [64] though this effect is relatively small as the transition temperature of α-Fe is well above of that of $La(Fe,Si)_{13}$ phase. For samples with a Si content of 1.5 ($LaFe_{11.5-x}Ni_xSi_{1.5}$), it was reported that their order of phase transition altered from FOPT to SOPT for alloys with a Ni content of x = 0.08 [26], which is a smaller limit compared to our case. Furthermore, a higher amount of 1:13 phase is attained for all samples studied in the present work.

The next method to determine the order of the phase transition using the field and temperature dependence of exponent n is model independent, unlike the previous technique [30]. It shows that a quantitative criterion of $n > 2$ near the transition indicates a FOPT and was successfully applied to different MC materials, such as $La(Fe,Si)_{13}$ and Heusler alloys, composites etc. From Fig. 8, overshoots of $n > 2$ near the phase transition for $LaFe_{11.6}Si_{1.4}$, $LaFe_{11.5}Ni_{0.1}Si_{1.4}$ and $LaFe_{11.4}Ni_{0.2}Si_{1.4}$ are observed, which indicate that they undergo FOPT. On the other hand, higher Ni-containing samples show a gradual increase from the minimum towards a maximum value of 2 (paramagnetic region), indicating SOPT behavior. This is in agreement with the previous observations in $n(T_{Trans})$ values.

In addition, the applicability of Banerjee's criterion to determine the order of phase transition [65] was also studied. This criterion establishes that the negative slopes of isothermal M^2 vs H/M curves (Arrott plots) indicate FOPT, while positive slopes point to SOPT. Furthermore, it implies that the material follows a mean field model. The Arrott plots of the studied samples are plotted in Fig. 9 (magnetic fields lower than 500 Oe are not considered). They show good agreement with the former analyses (from the exponent n) except for $LaFe_{11.4}Ni_{0.2}Si_{1.4}$ alloy, which shows positive slopes in the Arrott plot (instead of negative). One should note that this compound exhibits a composition very near to the compositional critical point of SOPT for this series (x = 0.21). The imposition of a mean field model in this method leads to values of the critical exponents rather different from those of the critical point of SOPT, which attributes to its failure for this composition ($LaFe_{11.4}Ni_{0.2}Si_{1.4}$). These were also reported for other magnetocaloric materials, wherein the results from Banerjee's criterion contradict to calorimetric data [66].

4. Conclusions

In this work, we studied the influence of Fe substitution by Ni on the structure, magnetic behavior and magnetocaloric effect of $La(Fe,Si)_{13}$ compounds. Using induction melting combined with suction casting, the required annealing duration was reduced by an order of magnitude as compared to that for the former counterparts. On top of that, the solid solubility of Ni in the desired 1:13 phase was extended. DFT calculations show that the $NaZn_{13}$-type structure was retained (Ni occupies the 96i sites) and only slight decrease in the overall magnetic moment was predicted (ascribed to the lower moment of Ni atoms); both theoretical predictions are in agreement with experimental results. Magnetocaloric studies show that the first order phase transition was transformed into a second order type with increasing Ni

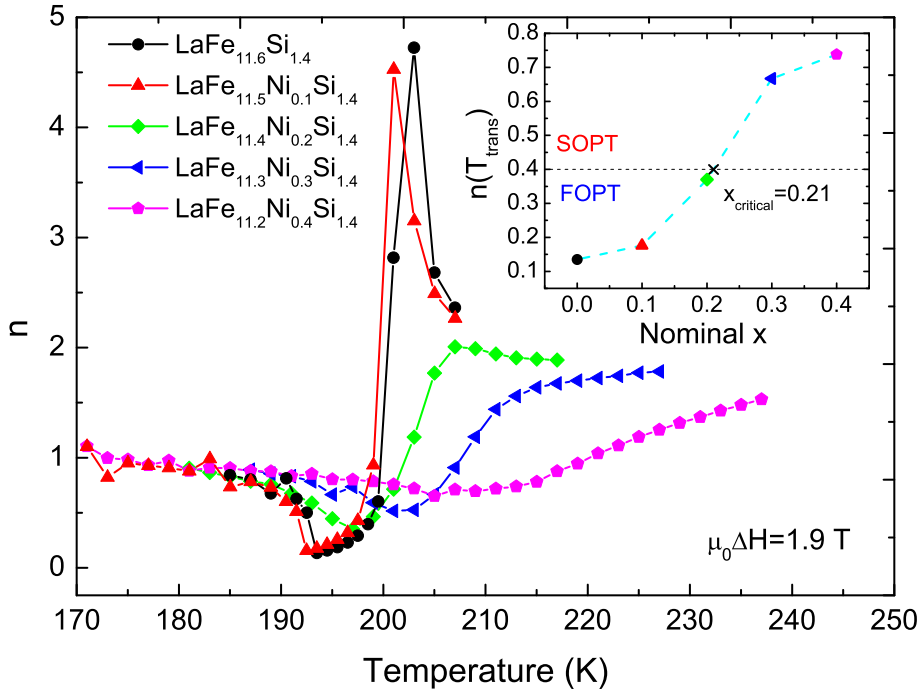

Fig. 8. Temperature dependence of the field dependence exponent n of ΔS_T (at $\mu_0\Delta H = 1.9$ T) for the $LaFe_{11.6-x}Ni_xSi_{1.4}$ series. Inset: n values at the transition temperature as a function of the Ni content.

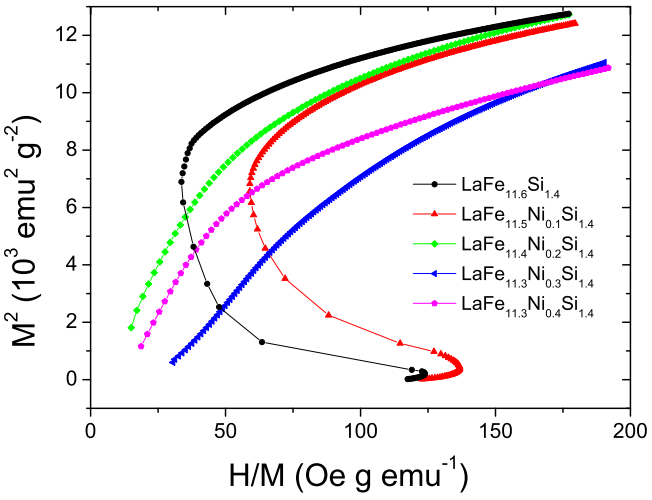

Fig. 9. Arrott plots for the $LaFe_{11.6-x}Ni_xSi_{1.4}$ series at selected temperatures close to their transitions.

concentration. We show that using the field dependence of magnetocaloric effect, the order of the phase transition can be unambiguously determined using a quantitative criterion even for compositions near the compositional critical point of SOPT (for which FOPT → SOPT). This critical point was determined as $x = 0.21$ in this work, leading to a 2.6-fold extension compared to previously reported similar alloys ($x = 0.08$) [26].

Acknowledgements

This work was supported by AEI/FEDER-UE (project MAT-2016-77265-R), the PAI of the Regional Government of Andalucía. L.M.R acknowledges a FPU fellowship from the Spanish MECD. C.R.M thanks Prof. Rubén Pérez and Dr. Pablo Pou for useful discussions. O.G., I.R., and K.S. acknowledge funding by the DFG in the framework of the priority program "Ferroic Cooling" (SPP1599).

References

[1] G.V. Brown, Magnetic heat pumping near room temperature, J. Appl. Phys. 47 (1976) 3673.
[2] O. Gutfleisch, M.A. Willard, E. Bruck, C.H. Chen, S.G. Sankar, J.P. Liu, Magnetic materials and devices for the 21st century: stronger, lighter, and more energy efficient, Adv. Mater. 23 (2011) 821.
[3] M. Balli, S. Jandl, P. Fournier, A. Kedous-Lebouc, Advanced materials for magnetic cooling: fundamentals and practical aspects, Appl. Phys. Rev. 4 (2017) 021305.
[4] V. Franco, J.S. Blázquez, J.J. Ipus, J.Y. Law, L.M. Moreno-Ramírez, A. Conde, Magnetocaloric effect: from materials research to refrigeration devices, Prog. Mater. Sci. 93 (2018) 112.
[5] C. Zimm, A. Jastrab, A. Sternberg, V. Pecharsky, K. Gschneidner, M. Osborne, I. Anderson, Description and performance of a near-room temperature magnetic refrigerator, Adv. Cryog. Eng. 43 (1998) 1759. Pts a and B 43.
[6] P. Weiss, A. Piccard, Le phénomène magnétocalorique, J. Phys. Theor. Appl. 7 (1917) 103.
[7] K.A. Gschneidner, V.K. Pecharsky, Magnetocaloric materials, Annu. Rev. Mater. Sci. 30 (2000) 387.
[8] E. Brück, Developments in magnetocaloric refrigeration, J. Phys. Appl. Phys. 38 (2005). R381.
[9] V. Franco, J.S. Blázquez, B. Ingale, A. Conde, The magnetocaloric effect and magnetic refrigeration near room temperature: materials and models, Annu. Rev. Mater. Res. 42 (2012) 305.
[10] J. Lyubina, Magnetocaloric materials for energy efficient cooling, J. Phys. Appl. Phys. 50 (2017) 053002.
[11] G. Jaeger, The ehrenfest classification of phase transitions: introduction and evolution, Arch. Hist. Exact Sci. 53 (1998) 51.
[12] O. Gutfleisch, T. Gottschall, M. Fries, D. Benke, I. Radulov, K.P. Skokov, H. Wende, M. Gruner, M. Acet, P. Entel, M. Farle, Mastering hysteresis in magnetocaloric materials, Philos. Trans. A. Math. Phys. Eng. Sci. 374 (2016), 20150308.
[13] J. Liu, J.D. Moore, K.P. Skokov, M. Krautz, K. Löwe, A. Barcza, M. Katter, O. Gutfleisch, Exploring La(Fe,Si)13-based magnetic refrigerants towards application, Scripta Mater. 67 (2012) 584.
[14] J. Lyubina, R. Schäfer, N. Martin, L. Schultz, O. Gutfleisch, Novel design of La(Fe, Si)(13) alloys towards high magnetic refrigeration performance, Adv. Mater. 22 (2010) 3735.
[15] K.H.J. Buschow, Intermetallic compounds of rare-earth and 3d transition metals, Rep. Prog. Phys. 40 (1977) 1179.
[16] K.H.J. Buschow, W.A.J.J. Velge, Phase relations and intermetallic compounds in

the lanthanum-cobalt system, J. Less Common Met. 13 (1967) 11.
[17] M.Q. Huang, W.E. Wallace, M.E. McHenry, Q. Chen, B.M. Ma, Soft magnetic properties of LaCo13 and La(Co, Fe)13 alloys, J. Appl. Phys. 83 (1998) 6471.
[18] M.Q. Huang, W.E. Wallace, R.T. Obermyer, S. Simizu, M. McHenry, S.G. Sankar, Magnetic characteristics of RCo13−xSix alloys (R=La, Pr, Nd, Gd, and Dy), J. Appl. Phys. 79 (1996) 5949.
[19] P.I. Krypiakewytsch, O.S. Zaretschniuk, E.I. Hladyschewskyj, O.I. Bodak, Ternre Verbindungen vom NaZn13-Typ, Z. Anorg. Allg. Chem. 358 (1968) 90.
[20] O. Gutfleisch, A. Yan, K.H. Müller, Large magnetocaloric effect in melt-spun LaFe13−xSix, J. Appl. Phys. 97 (2005), 10M305.
[21] V. Franco, J.Y. Law, A. Conde, V. Brabander, D.Y. Karpenkov, I. Radulov, K. Skokov, O. Gutfleisch, Predicting the tricritical point composition of a series of LaFeSi magnetocaloric alloys via universal scaling, J. Phys. Appl. Phys. 50 (2017) 414004.
[22] Z.-C. Wang, L.-H. He, F. Cuevas, M. Latroche, J. Shen, F.-W. Wang, Hydrogenation, structure and magnetic properties of La(Fe 0.91 Si 0.09) 13 hydrides and deuterides, Chin. Phys. B 20 (2011) 067502.
[23] I.A. Radulov, D.Y. Karpenkov, K.P. Skokov, A.Y. Karpenkov, T. Braun, V. Brabänder, T. Gottschall, M. Pabst, B. Stoll, O. Gutfleisch, Production and properties of metal-bonded La(Fe,Mn,Si)13Hx composite material, Acta Mater. 127 (2017) 389.
[24] B. Kaeswurm, V. Franco, K.P. Skokov, O. Gutfleisch, Assessment of the magnetocaloric effect in La, Pr(Fe, Si) under cycling, J. Magn. Magn Mater. 406 (2016) 259.
[25] M. Krautz, K. Skokov, T. Gottschall, C.S. Teixeira, A. Waske, J. Liu, L. Schultz, O. Gutfleisch, Systematic investigation of Mn substituted La(Fe,Si)13 alloys and their hydrides for room-temperature magnetocaloric application, J. Alloy. Comp. 598 (2014) 27.
[26] S.T. Zong, Y. Long, The influence of Cr and Ni on the character of magnetic phase transition in LaFe11.52-xMxSi1.48 alloys, AIP Adv. 8 (2017) 048101.
[27] G. Zsolt, Magnetic coupling in transition-metal–doped LaSiFe 11.5 TM 0.5 (TM=Cr, Mn, Co and Ni), Europhys. Lett. 110 (2015) 47006.
[28] M. Katter, V. Zellmann, G.W. Reppel, K. Uestuener, Magnetocaloric properties of La(Fe, Co, Si)(13) bulk material prepared by powder metallurgy, IEEE Trans. Magn. 44 (2008) 3044.
[29] C.P. Bean, D.S. Rodbell, Magnetic disorder as a first-order phase transformation, Phys. Rev. 126 (1962) 104.
[30] J.Y. Law, V. Franco, L.M. Moreno-Ramirez, A. Conde, D.Y. Karpenkov, I. Radulov, K.P. Skokov, O. Gutfleisch, A quantitative criterion for determining the order of magnetic phase transitions using the magnetocaloric effect, Nat. Commun. 9 (2018) 2680.
[31] B.G. Shen, J.R. Sun, F.X. Hu, H.W. Zhang, Z.H. Cheng, Recent progress in exploring magnetocaloric materials, Adv. Mater. 21 (2009) 4545.
[32] J. Lyubina, O. Gutfleisch, M.D. Kuz'min, M. Richter, La(Fe,Si)13-based magnetic refrigerants obtained by novel processing routes, J. Magn. Magn Mater. 321 (2009) 3571.
[33] V.K. Pecharsky, K.A. Gschneidner, Magnetocaloric effect from indirect measurements: magnetization and heat capacity, J. Appl. Phys. 86 (1999) 565.
[34] J. Liu, T. Gottschall, K.P. Skokov, J.D. Moore, O. Gutfleisch, Giant magnetocaloric effect driven by structural transitions, Nat. Mater. 11 (2012) 620.
[35] L. Tocado, E. Palacios, R. Burriel, Entropy determinations and magnetocaloric parameters in systems with first-order transitions: study of MnAs, J. Appl. Phys. 105 (2009) 093918.
[36] H. Oesterreicher, F.T. Parker, Magnetic cooling near Curie temperatures above 300 K, J. Appl. Phys. 55 (1984) 4334.
[37] V. Franco, A. Conde, Scaling laws for the magnetocaloric effect in second order phase transitions: from physics to applications for the characterization of materials, Int. J. Refrig. 33 (2010) 465.
[38] G. Kresse, J. Furthmüller, Efficient iterative schemes for ab initio total-energy calculations using a plane-wave basis set, Phys. Rev. B 54 (1996) 11169.
[39] M.E. Gruner, W. Keune, B. Roldan Cuenya, C. Weis, J. Landers, S.I. Makarov, D. Klar, M.Y. Hu, E.E. Alp, J. Zhao, M. Krautz, O. Gutfleisch, H. Wende, Element-resolved thermodynamics of magnetocaloric LaFe13-xSix, Phys. Rev. Lett. 114 (2015) 057202.
[40] M.E. Gruner, W. Keune, J. Landers, S. Salamon, M. Krautz, J. Zhao, M.Y. Hu, T. Toellner, E.E. Alp, O. Gutfleisch, H. Wende, Moment-volume coupling in La(Fe1−xSix)13, Physica Status Solidi (B) 255 (2018), 1700465.
[41] P.E. Blöchl, Projector augmented-wave method, Phys. Rev. B 50 (1994) 17953.
[42] G. Kresse, D. Joubert, From ultrasoft pseudopotentials to the projector augmented-wave method, Phys. Rev. B 59 (1999) 1758.
[43] J.P. Perdew, K. Burke, M. Ernzerhof, Generalized gradient approximation made simple, Phys. Rev. Lett. 77 (1996) 3865.
[44] H.J. Monkhorst, J.D. Pack, Special points for Brillouin-zone integrations, Phys. Rev. B 13 (1976) 5188.
[45] S.H. Vosko, L. Wilk, M. Nusair, Accurate spin-dependent electron liquid correlation energies for local spin density calculations: a critical analysis, Can. J. Phys. 58 (1980) 1200.
[46] C.L. Wang, Y. Long, Magnetic properties and magnetocaloric effect of LaFe11.5−xTxSi1.5 (T = Cr, Ni), J. Appl. Phys. 113 (2013) 143902.
[47] S.T. Zong, C.L. Wang, Y. Long, B. Fu, J.M. Shi, J. Han, Y.Y. Zhao, Solid solubility in 1:13 phase of doping element for La(Fe,Si)13 alloys, AIP Adv. 6 (2016) 056223.
[48] W. Fangwei, W. Guang-jun, H. Feng-xia, A. Kurbakov, S. Bao-gen, C. Zhao-hua, Strong interplay between structure and magnetism in the giant magnetocaloric intermetallic compound LaFe 11.4 Si 1.6 : a neutron diffraction study, J. Phys. Condens. Matter 15 (2003) 5269.
[49] M. Rosca, M. Balli, D. Fruchart, D. Gignoux, E.K. Hlil, S. Miraglia, B. Ouladdiaf, P. Wolfers, Neutron diffraction study of LaFe11.31Si1.69 and LaFe11.31-Si1.69H1.45 compounds, J. Alloy. Comp. 490 (2010) 50.
[50] A. Fujita, H. Yako, Stability of metallic, magnetic and electronic states in NaZn13-type La(FexSi1−x)13 magnetocaloric compounds, Scripta Mater. 67 (2012) 578.
[51] F. Wang, A. Kurbakov, G.-J. Wang, F.-X. Hu, B.-G. Shen, Z.-H. Cheng, Strong interplay between structure and magnetism in LaFe11.3Co0.6Si1.1: a neutron diffraction study, Phys. B Condens. Matter 385–386 (2006) 343.
[52] T.T.M. Palstra, J.A. Mydosh, G.J. Nieuwenhuys, A.M. van der Kraan, K.H.J. Buschow, Study of the critical behaviour of the magnetization and electrical resistivity in cubic La(Fe, Si)13 compounds, J. Magn. Magn Mater. 36 (1983) 290.
[53] J.M.D. Coey, Magnetism and Magnetic Materials, vol. 150, Cambdrige University Press, 2009.
[54] M. Hatherly, K. Hirakawa, R.D. Lowde, J.F. Mallett, M.W. Stringfellow, B.H. Torrie, Spin wave energies and exchange parameters in iron-nickel alloys, Proc. Phys. Soc. 84 (1964) 55.
[55] I. Yang, S.Y. Savrasov, G. Kotliar, Importance of correlation effects on magnetic anisotropy in Fe and Ni, Phys. Rev. Lett. 87 (2001) 216405.
[56] F.-X. Hu, X.-L. Qian, G.-J. Wang, J.-R. Sun, B.-G. Shen, Z.-H. Cheng, J. Gao, Magnetoresistances and magnetic entropy changes associated with negative lattice expansions in NaZn 13 -type compounds LaFeCoSi, Chin. Phys. 14 (2005) 2329.
[57] F.X. Hu, J. Gao, X.L. Qian, M. Ilyn, A.M. Tishin, J.R. Sun, B.G. Shen, Magnetocaloric effect in itinerant electron metamagnetic systems La(Fe1−xCox) 11.9Si1.1, J. Appl. Phys. 97 (2005), 10M303.
[58] F. Guillou, H. Yibole, G. Porcari, L. Zhang, N.H. van Dijk, E. Brück, Magnetocaloric effect, cyclability and coefficient of refrigerant performance in the MnFe(P, Si, B) system, J. Appl. Phys. 116 (2014) 063903.
[59] K. Huang, Statistical Mechanics, second ed., John Wiley & Sons, 1987.
[60] C. Romero-Muniz, V. Franco, A. Conde, Two different critical regimes enclosed in the Bean-Rodbell model and their implications for the field dependence and universal scaling of the magnetocaloric effect, Phys. Chem. Chem. Phys. 19 (2017) 3582.
[61] R. Caballero-Flores, V. Franco, A. Conde, L.F. Kiss, Influence of the demagnetizing field on the determination of the magnetocaloric effect from magnetization curves, J. Appl. Phys. 105 (2009), 07A919.
[62] C. Romero-Muñiz, J.J. Ipus, J.S. Blázquez, V. Franco, A. Conde, Influence of the demagnetizing factor on the magnetocaloric effect: critical scaling and numerical simulations, Appl. Phys. Lett. 104 (2014) 252405.
[63] L.M. Moreno-Ramírez, J.J. Ipus, V. Franco, J.S. Blázquez, A. Conde, Analysis of magnetocaloric effect of ball milled amorphous alloys: demagnetizing factor and Curie temperature distribution, J. Alloy. Comp. 622 (2015) 606.
[64] J.S. Blázquez, L.M. Moreno-Ramírez, J.J. Ipus, L.F. Kiss, D. Kaptás, T. Kemény, V. Franco, A. Conde, Effect of α-Fe impurities on the field dependence of magnetocaloric response in LaFe11.5Si1.5, J. Alloy. Comp. 646 (2015) 101.
[65] B.K. Banerjee, On a generalised approach to first and second order magnetic transitions, Phys. Lett. 12 (1964) 16.
[66] C.M. Bonilla, J. Herrero-Albillos, F. Bartolomé, L.M. García, M. Parra-Borderías, V. Franco, Universal behavior for magnetic entropy change in magnetocaloric materials: an analysis on the nature of phase transitions, Phys. Rev. B 81 (2010) 224424.